INTERNATIONAL JOURNAL OF FLUID POWER, 2016
VOL. 17, NO. 2, 90–101
http://dx.doi.org/10.1080/14399776.2016.1141636

Taylor & Francis
Taylor & Francis Group

Modelling and experimental validation of a nonlinear proportional solenoid pressure control valve

Alessandro Dell'Amico and Petter Krus

Division of Fluid and Mechatronic Systems, Department of Management and Engineering, Linköping University, Linköping, Sweden

ABSTRACT

This paper investigates the static and dynamic behaviour of a pressure control valve with nonlinear negative characteristics. The pressure control valve has both reducing and relieving capability and is actuated by a solenoid. The static characteristics have been measured over the entire working range, covering the dynamic response of the solenoid, as well as the complete valve. A model is proposed that considers the flow as a mix of laminar and turbulent flow and flow forces with a flow angle that varies with the stroke of the spool. The model shows good agreement with measurements. The investigations show that the flow forces decrease with higher flow rates as a result of a flow angle that tends to go towards a vertical angle. This results in an increase in pressure with flow during pressure reducing mode. A linear analysis is also presented, explaining this as a negative spring constant in the low frequency range. Stability is, however, maintained.

ARTICLE HISTORY
Received 17 October 2015
Accepted 24 December 2015

KEYWORDS
Nonlinear modelling; solenoid; pressure control valve; linear analysis

1. Introduction

A pressure control valve is one of the most common components in any hydraulic system. Usually it is in the form of a pressure relief valve, keeping the maximum allowed pressure in the system to a defined value. The other type of pressure control valve is the pressure reducing valve, designed to maintain a certain pressure regardless of the inlet pressure. A proportional pressure control valve is a combination of the two. As it is actuated by a solenoid, the pressure is proportional to the current. These valves can be found in typical applications such as automatic gearboxes and as pilot stages for spool valves.

In a closed-centre electro-hydraulic power steering system, see Dell'Amico (2013), such a valve could serve as an interesting solution. The main purpose of a power assisted steering system is to reduce the driver's workload when turning the steering wheel. This is done by controlling the level of assistive pressure with a hydro-mechanical open-centre valve. By replacing the open-centre valve with proportional pressure control valves with closed-centre, the solution offers the possibility to realise active steering or automatic control of vehicles as it also reduces energy consumption.

As for all pressure control valves, these come both as single stage valves and two-stage valves, where the former is simple in its construction and much cheaper. Its performance is, however, limited by the size of the valve and especially the electro-mechanical actuator, the solenoid. A two-stage valve usually has very good static characteristics. Due to mainly cost and packaging properties, the single stage valve is considered in this work. A potential candidate is the Hydac PDR08-11 proportional pressure control valve, which is primarily designed as a pilot stage for a spool valve. Measurements show non-typical behaviour, where the pressure reducing curves have negative static characteristics, i.e. a positive slope in the flow-pressure curve. This suggests that it is important to consider in detail the flow-pressure relationship and flow forces of the valve, as well as the solenoid's characteristics when modelling the valve. These subjects have all been investigated by several researchers. In control design, it is important to have a clear overview of the valve and a detailed model will be beneficial.

Merritt (1967) gives a good overview of different types of fluid flow. The flow is usually turbulent and the discharge coefficient can be assumed to be a constant value. The flow is then proportional to the square root of the pressure drop. In cases where the flow is more laminar, the discharge coefficient is instead modelled as a function of the square root of the Reynolds number. In a strict laminar case, this yields that the flow is directly proportional to the pressure drop. If a pure square root model is assumed, numerical issues can be encountered at very low pressure drops since the derivative tends to go to infinity. Ellman and Piché (1996) propose a two-region flow model in order to handle this. This is also done by Åman *et al.* (2008), who use a cubic spline curve for the laminar and transition region. This method has proven to be computationally effecient compared to the traditional orifice flow model. Another way is proposed by Wu *et al.* (2002), where an exponential model of the discharge coefficient as a function of the Reynolds number is used. Since the Reynolds number itself is

CONTACT Alessandro Dell'Amico alessandro.dellamico@liu.se

dependent on the flow, this model requires an iterative process or a pre-defined look-up table to solve. The flow can also be divided into a linear term and a nonlinear term. This is adapted by Borutzky *et al.* (2002) where a single formula for the discharge coefficient is proposed, with purpose to handle the numerical effeciency. This results in a linear and a quadratic term in the pressure flow relation.

The flow forces of the open-centre directional valve were measured and analysed by Amirante *et al.* (2006). Depending on the position of the spool, the flow forces initially act to open the valve, whereas they change direction to close the valve after a certain opening. Stationary flow forces were also analysed on compensated spool valves by Borghi *et al.* (2000). Computional Fluid Dynamics (CFD) was used to analyse the jet flow angle and the flow forces in general for different designs. These works show that the general assumption of a static jet stream angle is far from the reality in some cases and which should be considered.

Pressure control valves in different configuration have been investigated and analysed by several researchers. Merritt (1967) provides an analysis of single stage pressure relief and reducing valves, with a focus on the dynamic response. A pilot-controlled solenoid pressure relief valve is modelled and analysed using the bondgraph technique by Dasgupta and Watton (2005). With a simplified model of the solenoid, the paper presents a good model of the valve. A more detailed model of a solenoid is presented by Vaughan and Gamble (1996). By measuring the current and voltage of the solenoid, the magnetization curves can be derived, which also include hysteresis effects. A direct acting solenoid valve for cluctch control is modelled and analysed by Walker *et al.* (2014). A nonlinear detailed model, where the solenoid characteristics are mapped, is presented. The model agrees well with both step inputs and steady state. A PWM-driven solenoid for ABS valves is modelled by Branciforte *et al.* (2011). The fast dynamics are modelled using a fractional order system, while the hysteresis is covered by using neural networks. A general linearised analysis of a pressure relief valve is presented in Palmberg *et al.* (1983). It is shown how most valves can be characterised by a dominating break frequency and compliance and the system being connected to the valve by the hydraulic capacitance and the flow-pressure coefficient. This was also verified by experiments. A design process for a proportional pressure relief valve is proposed by Erhard *et al.* (2013). An inverse simulation technique is used to derive a design for both the hydraulic subsystem and the solenoid characteristics. The valve is simulated using both CFD for the hydraulic subsystem and the Finite Element Method for the solenoid. What can be seen is that different approaches exists to model and analyse the valve depending on the purpose. In this work a 1-D model and simulation for both the solenoid and hydraulic is adapted, which facilitates the analysis and future control design.

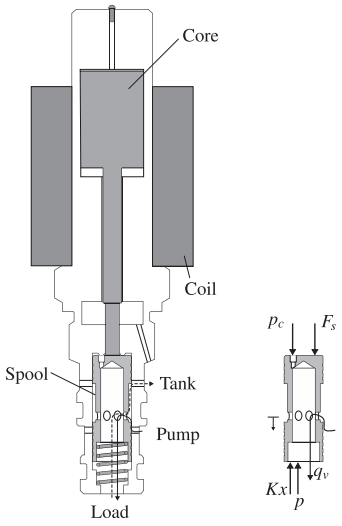

Figure 1. Simplified schematic of the valve. Solid flow path is from pump to load. Dashed flow path is from load to tank. Forces acting on the spool are also shown.

The main aim of this paper is to find a suitable model that explaines the negative characteristics of the valve. The model is divided into two subsystems: the solenoid and the hydro-mechanical subsystems. An orifice flow model is proposed that covers laminar to turbulent flow without requiring an iterative solution. The flow forces are also modelled considering how the flow jet angle changes over the spool stroke. Experiments have been conducted for both static and dynamic measurements for both the solenoid and the complete valve and compared to the simulation results. A linear analysis of the system is also presented that explaines the valve's behaviour.

2. System description

The main purpose of the valve is to maintain a certain pressure corresponding to the input signal regardless of variation in the load flow and supply pressure. However, this is only true in the ideal case and the static characteristics of the valve determine how much the pressure will fluctuate with variations in for example flow. The input signal is a PWM-modulated voltage, but typically it is the current that is of interest. A certain current will correspond to a certain static pressure level. Obviously, the valve can take different shapes with the same functionality. A simplified schematic of the valve studied in this paper is shown in Figure 1. Parameter data can be found in Table 1 in the appendix.

The valve is a direct acting single-stage valve. This means that an electro-magnetic actuator, a solenoid, exerts a force directly on the spool of the valve. In the opposite direction to the solenoid force, the load pressure acts on a predefined surface, together with a small

spring. The reference pressure is thus modulated by the solenoid force. Once the load pressure has reached the reference pressure, the spool will be in equilibrium. If no load flow is required, the spool will be in the closed position and no flow is going through the valve except for leakage. If the load pressure becomes lower than the corresponding reference pressure, the spool opens to pump, like a reducing valve. If the pressure is too high, the spool opens to tank to reduce the pressure, like a relief valve. The valve is therefore self-regulating.

A small restrictor is placed between the load volume and a much smaller volume above the spool. This solution serves to increase the damping. A further analysis of the restrictor is presented below which reveals its true impact on the valve. The opening areas of the valve consists at the pump side of 12 circular holes around the valve body, each with a diameter of 1.5 mm. On the tank side, there are also 12 holes in the same manner. However, a single small hole of 0.8 mm diameter is placed before the larger holes with an offset of 0.3 mm. This generates a much smoother area gradient on the tank side compared to the pump side.

With the centre position of the spool at 0 mm, the spool's stroke is from −1 to 0.85 mm. The core's stroke is approximately from −1.7 to 0.85 mm.

3. Experimental setup

The measurements of the valve have been divided into two parts. The first part studies the solenoid separately to get a good overview of its behaviour. The other part studies the complete valve, both static and dynamic characteristics. Two test rigs were set up for this purpose. All measurements were conducted with a sample time of 0.1 ms. A PWM-modulated signal at 200 Hz was used to control the valve. The voltage and current were filtered using an FIR filter to remove the effect of the PWM-signal on the measurements. The results of all measurements are the foundation for the modelling procedure in Section 4.

3.1. Solenoid measurements

A low-speed electro-mechanical actuator with a load cell attached to its end was used to control the position of the magnet core. The solenoid was clamped such that the core was resting against the load cell in the horizontal position. The solenoid was supplied with 12 V. Two types of test were conducted. The first applied step input signals at 25 different positions over the entire stroke. The voltage, current and force were measured. The other tests measured the static relationship between current and force. Since the core was only resting against the load cell and no spring was used, no PWM-modulation was used to avoid oscillations of the core. Instead, the supply voltage was slowly increased while current and force were registered. Before each test

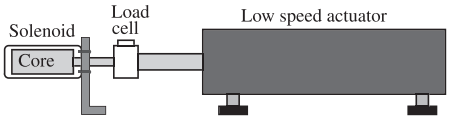

Figure 2. A schematic of the measurement set-up of the solenoid.

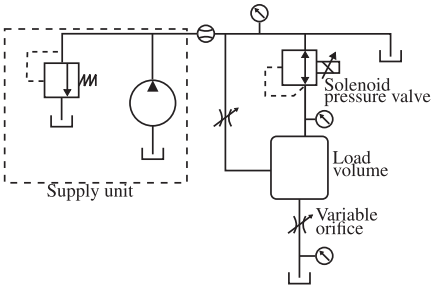

Figure 3. A schematic of the measurement set-up of the complete valve.

the solenoid was heated by applying maximum current to avoid fluctations in the coil resistance. A schematic of this test rig is shown in Figure 2. The static behaviour of the solenoid is shown in Figure 8, which demonstrates the strong nonlinear nature of the solenoid. The results from the second type of test, are shown in Figure 9.

3.2. Valve measurements

The test rig for measurements of the complete valve is illustrated in Figure 3. The valve is connected to a constant pressure source at 200 bar. A small accumulator of 1 L is installed to minimise variations in the supply pressure. The load consists of a fixed volume of 0.1 L. A flow-meter is installed on the supply line, as well as a temperature sensor. The temperature varied between 37 and 42 °C for all tests. Two variable orifices are installed, one between the load volume and tank and the other between the pump and load volume. These are used to apply a positive or negative load flow. Load, supply and tank pressures are measured with transducers. The magnet core housing is fitted with a small screw at its end. The screw is used to bleed the core housing, since it is filled with oil. When removed, the hole gives access to the magnet core. A position transducer was installed to measure the core position. As long as the core is in contact with the spool, the core position corresponds to the spool position. The position transducer is spring-loaded to ensure it is always in contact with the core, at the same time as the spring force is kept low enough to have no impact on the valve.

To measure the static characteristic of the valve, a constant duty cycle was applied. Either of the two variable orifices was slowly opened to increase the load flow, while pressure, flow and spool position were registered. This was done from 30 to 100% duty cycle with steps of 10%, both for positive and negative load flow, i.e. the

valve is working either as a reducing valve or a relief valve. The measured static characteristics are shown in Figure 10.

When measuring the dynamic characteristic, the load flow was set at zero. Steps were applied in the input signal for different levels and amplitudes, while pressure, current and spool position were registered. If too sudden an input signal was applied when relieving the pressure, the magnet core and spool could separate and cause great undershots in the pressure. This was clearly seen by measurements. Since this is an unwanted behaviour and is outside the scope of this paper, a rate limiter is implemented for a decreasing input signal. The rate limiter is tuned so that the core and spool stay in contact. The dynamic behaviour of the valve is shown in Figure 11.

4. Modelling

The modelling procedure for the valve is divided into two parts, where the solenoid and hydraulic subsystems are modelled separately.

4.1. Solenoid model

Since magnetic properties are difficult to measure and no further properties of the magnet are available, the modelling procedure for the solenoid is based on the work done by Vaughan and Gamble (1996). It only requires measurements of the current, voltage and force, which are much easier to accomplish and which are used to derive the magnetic characteristic. The idea is to model the solenoid as a resistor in series with a nonlinear inductor, while also considering magnetic hysteresis. The total voltage over the solenoid consists of a resistive part and an inductive part, as in Equation (1),

$$V_s = V_R + V_L = iR + V_L \tag{1}$$

where V_S is the total voltage over the solenoid, V_R is the resistive voltage drop, V_L is the inductive voltage drop, i is the current through the coil and R is the coil resistance. The current is described as an energy-restoring part, i_R, and an energy-dissipating part, i_d, and describes the magnetic characteristics, Equation (2).

$$i = i_R + i_d = f(\lambda, x) + d(V_L) \tag{2}$$

The restoring function depends on both the flux linkage λ and the core position x, while the dissipating function depends only on the inductive voltage. The flux linkage can easily be obtained through Equation (3). The magnetic characteristic is usually desribed by the so called magnetization curve. One way to derive this curve is through the flux linkage and current. The calculated magnetization curves are shown in Figure 9(a).

$$\lambda = \int V_L = \int \left(V_s - iR\right) \tag{3}$$

The restoring function is found by calculating the mean current from the magnetization curves at each core position and fitting a polynomial function. The best fit for this solenoid is described by Equation (4)–(7).

$$i_R = f_1\lambda^3 + f_2\lambda^2 + f_3\lambda \tag{4}$$

$$f_1 = p_{f_{11}}x^5 + p_{f_{12}}x^4 + p_{f_{13}}x^3 + p_{f_{14}}x^2 + p_{f_{15}}x + p_{f_{16}} \tag{5}$$

$$f_2 = p_{f_{21}}x^5 + p_{f_{22}}x^4 + p_{f_{23}}x^3 + p_{f_{24}}x^2 + p_{f_{25}}x + p_{f_{26}} \tag{6}$$

$$f_3 = p_{f_{31}}x^2 + p_{f_{32}}x + p_{f_{33}} \tag{7}$$

The dissipating function is also fitted with a polynomial from the calculated dissipating current, with a best fit as in Equation (8).

$$i_d = p_{d_1}V_L^3 + p_{d_2}V_L^2 + p_{d_3}V_L + p_{d_4} \tag{8}$$

Values of all constants can be found in Table 1. The solenoid force is modelled as a function $F_s(i, x)$ of the current and the core position, since it was practical to measure the static relationship for each core position. Again a polynomial model is fitted, described in Equations (9)–(12).

$$F_s(i,x) = p_{fs1}i^5 + p_{fs2}i^4 + p_{fs3}i^3 + p_{fs4}i^2 \tag{9}$$

$$p_{fs1} = p_{fs11}x^3 + p_{fs12}x^2 + p_{fs13}x + p_{fs14} \tag{10}$$

$$p_{fs2} = p_{fs21}x^3 + p_{fs22}x^2 + p_{fs23}x + p_{fs24} \tag{11}$$

$$p_{fs3} = p_{fs31}x^3 + p_{fs32}x^2 + p_{fs33}x + p_{fs34} \tag{12}$$

$$p_{fs4} = p_{fs41}x^3 + p_{fs42}x^2 + p_{fs43}x + p_{fs44} \tag{13}$$

The static characteristic of the solenoid is only modelled for the working range of the valve, which is from 1 mm to maximum position of the core. The comparison to the measured characteristic is shown in Figure 8, while a comparison of the dynamic behaviour can be found in Figure 9.

4.2. Hydraulic model

Studying the results from the measurements, in particular the static characteristic of the valve in Figure 10, a few things can be concluded that will form the model of the valve. Firstly, it can be seen that the spool works with an offset from the centre position towards the tank side at equilibrium, i.e. a negative stroke. This is due to the difference in area gradient and pressure drop over the meter-in and meter-out orifices. To cover the leakage from the pump side, the valve needs to open somewhat to tank. It is therefore important to consider this when modelling the valve. It is done by regarding both the gap leakage and area opening on the pump side as two orifices, each with different characteristics. The gap leakage on the tank side is less important due to the smoother area gradient.

The second thing concluded is that generally the valve is working with low flows. It is far from certain that the flow reaches fully turbulent flow and the common assumption that the discharge coefficient is constant might be far from the truth. This is checked by calculating the discharge coefficient from measurements. Obviously, the discharge coefficient is not purely a physical property and any assumption and modelling mismatch will affect its behaviour.

Thirdly, the static characteristic of the valve is very specific when working as a pressure-reducing valve. As can be seen in Figure 10, the pressure begins to increase for larger flows, which is not the expected behaviour of a pressure-reducing valve. The typical behaviour of a solenoid is an increased force with stroke, i.e. for a smaller air gap, which is also seen in Figure 8. The increase in force, however, is too small to fully explain the increase in pressure. It is left to the flow forces to explain the behaviour.

The equations describing the hydraulic part of the valve in reducing mode are as in Equations (14)–(32). When relieving the pressure, the modelling procedure is the same.

Spool motion

$$m\dot{v} = F_s(i,x) - A_c p + A_{cc} p_c - Kx - Bv - F_f(x,\Delta p) - f_0 \tag{14}$$

Here m is the total moving mass, A_c the pressure area, A_{cc} is the damping chamber area, p is the load pressure, p_c the pressure in the damping chamber, K the spring stiffness, B the viscous friction coefficient, v the mass velocity, $F_f(x,\Delta p)$ the flow force and f_0 the spring pretension force. Only viscous friction is considered. Static friction and stick-slip phenomena are assumed to be negligible due to the dither effect of the PWM input. The spool's stroke is limited between −0.55 and 0.85 mm, which according to measurements is the interesting working range.

Continuity equation

$$q_v - q_c - q_l = \frac{V}{\beta}\dot{p} \tag{15}$$

where q_v is the flow through the valve, q_c the flow into the damping chamber, q_l the load flow, V the load volume and p the load pressure.

Orifice flow

$$q_v = C_q(x,\Delta p)A(x)\sqrt{\frac{2}{\rho}\Delta p} \tag{16}$$

where Δp is the pressure drop over the orifice, C_q the discharge coefficient and $A(x)$ the opening area. On the pump side, the valve is modelled with two orifices, one for the gap leakage and the other when the spool passes the holes. In Equation (16), which assumes turbulent flow, is used in both cases. The opening area is modelled according to Equation (17), which considers the 12 circular holes and a plane leakage gap at each hole. On the tank side, the opening area is modelled in the same manner but also considering the small initial hole.

$$A(x) = 12\left(\frac{1}{2}r^2\left(2arccos\left(\frac{r - x\cdot 10^{-3}}{r}\right) - sin\left(2arccos\left(\frac{r - x\cdot 10^{-3}}{r}\right)\right)\right) + 2rh_{gap}\right) \tag{17}$$

Here r is the radius of one hole and h_{gap} the height of the gap. Since the flow can be anything from laminar to turbulent, the discharge coefficient C_q is modelled to take this into account. The discharge coefficient can be calculated from Equation (16) and using the data from Figure 10 and is shown in Figure 4(a) for the pump side and in Figure 4(b) for the tank side. The discharge coefficient is split into two parts. For gap leakage, the flow is assumed proportional to the pressure drop. According to the literature, Merritt (1967), the discharge coefficient is proportional to the square root of the Reynolds number R_e, which is calculated according to Equation (18),

$$R_e = \frac{qd_h}{A\nu} \qquad d_h = \frac{4A}{O}$$
$$\Rightarrow R_e = \frac{4q}{O\nu} \tag{18}$$

where d_h is the hydraulic diameter, ν the kinematic viscosity and O the circumference of the opening. The discharge coefficient for the gap leakage is then modelled as in Equation (19).

$$C_{q_{gap}} = g_g(x)\sqrt{R_e} \tag{19}$$

The function $g_g(x)$ is a geometrical term that will both compensate for any errors in the area opening function and take into account the effective cross area of the fluid stream. Studying the discharge coefficient it can be seen that the value tends to approach a constant value when the spool crosses the holes at 0 mm. The flow goes from laminar to a mix of laminar and turbulent flow as the spool opens more. The discharge coefficient is no longer proportional to the square root of the Reynolds number and a more complicated relation would require an iterative process to solve. This is not practical when implementing the model in simulation software. In this case, the discharge coefficient is instead modelled as in Equation (20), where it only depends on the spool position and pressure.

$$C_{q_{hole}}(x,p) = g(x)p^{\gamma(x)} \tag{20}$$

The function $g(x)$ is again a geomentrical term, while $\gamma(x)$ handles the transition from laminar to turbulent

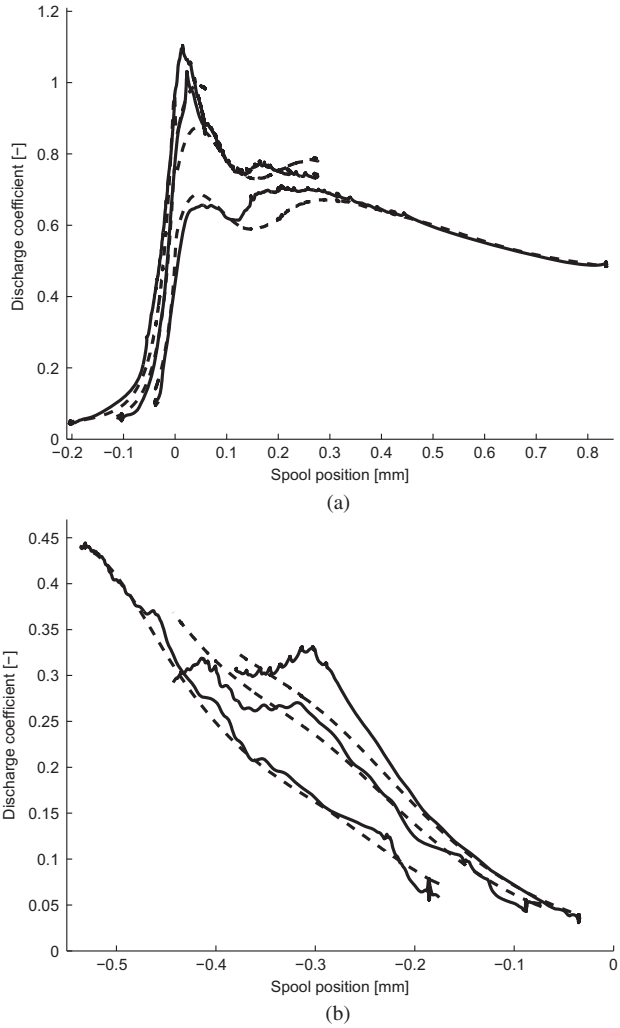

Figure 4. Measured (solid) and simulated (dashed) discharge coefficient for the pump side (a) and tank side (b) at corresponding 30, 60 and 90% duty cycle.

flow and varies between 0 and 0.5. An arctan function, which was manually tuned, was used in this paper and the three functions $\gamma(x)$, $g_g(x)$ and $g(x)$ are described in Equation (21)–(22). The geometrical functions are derived by using an appropriate curve fitting technique.

$$g_g(x) = 0.02477e^{1.314x} + 0.0642e^{24.41x} \quad (21)$$

$$\begin{aligned} g(x) = {} & 0.3973sin(3.493x - 0.6221) \\ & + 3.789sin(6.942x + 1.088) \\ & + 3.626sin(7.047x + 4.173) \\ & + 0.0009295sin(22.45x + 2.653) \end{aligned} \quad (22)$$

$$\gamma(x) = ((-arctan(5(x - 0.3))) + \pi/2)0.3/\pi \quad (23)$$

The gap leakage on the tank side is assumed to be very small due to the smoother area gradient and no separate measurements of it were recorded. It is therefore lumped together with the main flow and the pressure-flow characteristic is modelled with the same method as on the tank side, resulting in the functions $\gamma_r(x)$ and

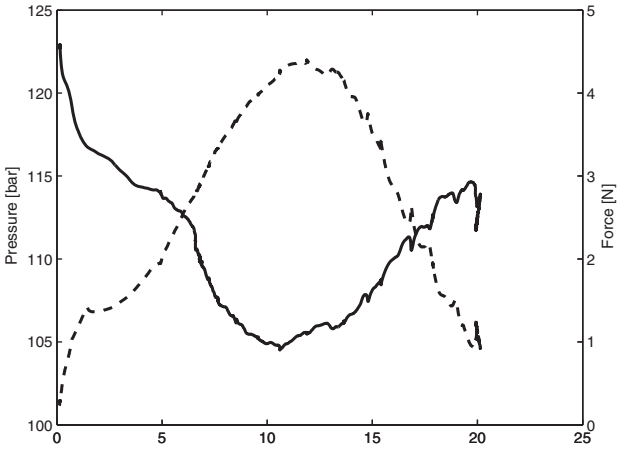

Figure 5. Measured pressure (solid) and calculated flow force (dashed) vs. the flow at 70% duty cycle.

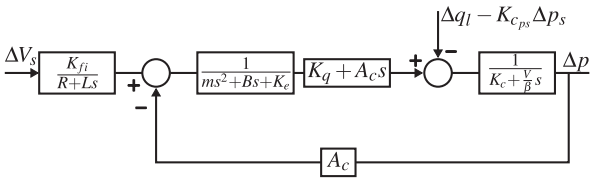

Figure 6. Block diagram of the linearised valve equations.

$g_r(x)$ and shown in Equations (24) and (25).

$$g_r(x) = 0.1267e^{-\frac{|x|-0.5556^2}{0.1016}} + 10880e^{-\frac{|x|-3.269^2}{0.7823}} \quad (24)$$

$$\gamma_r(x) = ((-arctan(10(|x| - 0.4))) + \pi/2)0.3/\pi \quad (25)$$

The resulting functions are also plotted in Figures 4(a) and 4(b). The logistic function, Equations (26) and (27), is used on the pump side to get a smooth continuous transition from the gap to the holes.

$$C_q = C_{q_{gap}} \cdot (1 - L(x)) + C_{q_{hole}} \cdot L(x) \quad (26)$$

$$L(x) = \frac{1}{1 - e^{1000x}} \quad (27)$$

Damping orifice and chamber

$$q_c = K_d(p - p_c) \quad (28)$$

$$q_c - A_{cc}v = \frac{V_c}{\beta}\dot{p}_c \quad (29)$$

where V_c is the volume of the damping chamber. The flow into the damping chamber q_c, Equations (28) and (29), not only depends on the size of the damping orifice but also on the leakage flow over the spool land. This flow is assumed to be laminar and is modelled with the constant K_d, which is tuned to give a good match with measurements.

Flow forces

Since the mechanical spring is very weak, the static characteristic of the valve is mainly defined by the flow

Table 1. The working points for frequency analysis.

	i	x_v	p
Point 1	1.5 [A]	-0.0326 [mm]	120.4 [bar]
Point 2	1.49 [A]	0.2482 [mm]	109.6 [bar]

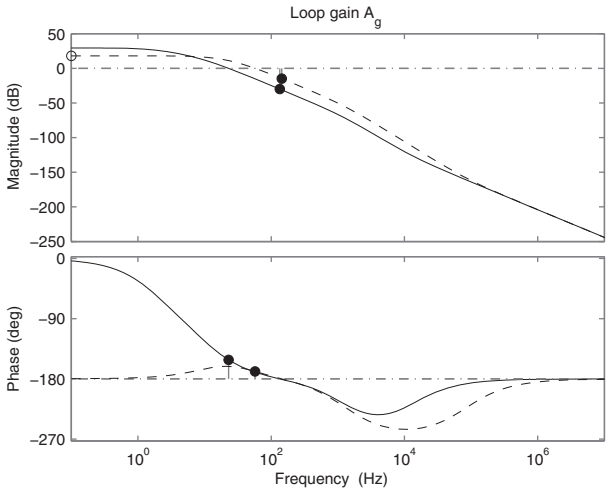

Figure 7. Loop gain frequency response of the valve. The solid line corresponds to working point 1 and the dashed lines corresponds to working point 2. The dots indicate the gain and phase margins, respectively.

forces. The flow forces are defined in Equation (30), where only stationary flow forces are considered.

$$F_f(x, \Delta p) = 2C_q(x, \Delta p)A(x)\Delta p cos(\delta) \tag{30}$$

Since the discharge coefficient is known, the flow angle δ can be calculated from the spool equilibrium in Equation (14). The models used in this paper are defined in Equations (31) and (32) and are derived by using an appropriate curve fitting technique.

Pump side

$$cos(\delta) = max\left(0.7, 6.151 \cdot 10^{13} e^{-\frac{x+3.129}{0.5478}^2} + 0.1908 e^{-\frac{x-0.154}{0.106}^2}\right) \tag{31}$$

Tank side

$$cos(\delta) = max\left(0.7, 932 e^{-\frac{|x|+1.741}{0.7617}^2} + 0.3796 e^{-\frac{|x|-0.5226}{0.2083}^2}\right) \tag{32}$$

Note that for convenience the cosine of the flow angle is modelled rather than the flow angle itself. The resulting flow force at 70% duty cycle is shown in Figure 5, together with the corresponding pressure. It can be seen how the flow forces begins to decrease at a certain level, which results in an increase in pressure. Static and dynamic comparisons between measurements and the implemented model are shown in Section 6.

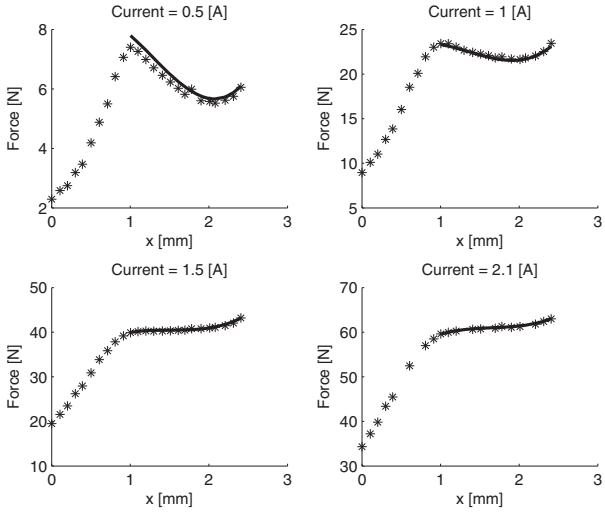

Figure 8. Measured and modelled (solid line) static characteristic of the solenoid plotted as force vs. position. 0 mm corresponds to the core's end position, where a positive direction closes the air gap.

4.3. Simplified model

The effect of the damping chamber and restrictor has been analysed by Merritt (1967). If the restrictor is small enough, it will serve to trap the oil in the damping chamber, effectively replacing the mechanical resonance with a hydraulic resonance and adding a low-frequency lag. The effect of this is increased stability. In order for this to be valid, the restrictor must fulfill the criteria in Equation (33).

$$K_d \geq 2A_c\sqrt{\frac{V_c}{m\beta}} \tag{33}$$

With the values in Table 1, for this valve the restrictor does not fulfil the criteria. According to Merritt (1967), the effect of the restrictor is instead an increased damping on the mechanical resonance. This also implies that the valve can be simplified by removing one state, i.e. the damping chamber and restrictor. The simplified model is compared to the full model and the mechanical damping is tuned to obtain a good fit. It is advantageous to run the model with the simplified model. It is not as stiff as the full model and does not require as low step time during simulation.

5. Linear modelling and frequency analysis

A linear model and analysis is helpful when studying the system and reveals some important behaviour. The following analysis is based on the simplified model explained in Section 4.3 and considers only the pressure-reducing case. A frequency analysis requires the system to be linear and the first step is to linearise the system equations from Section 4. Here the pressure p_c is set to p since the damping chamber is ignored. Since the static characteristic of the valve is mainly due to the hydraulic

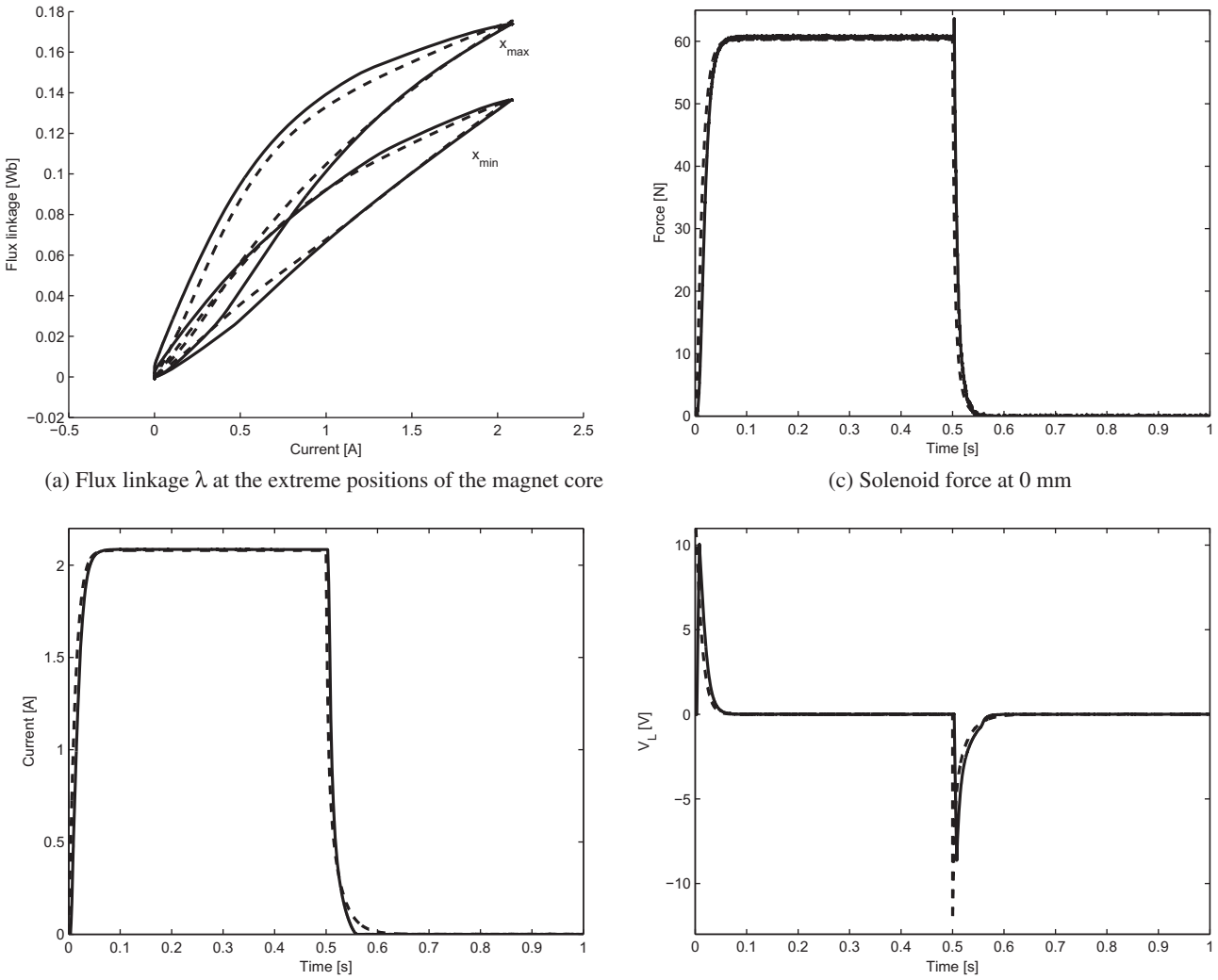

(a) Flux linkage λ at the extreme positions of the magnet core

(c) Solenoid force at 0 mm

(b) Solenoid current at 0 mm

(d) Inductive voltage at 0 mm

Figure 9. Comparisons between measurement (solid) and simulation (dashed) results of the solenoid for step responses.

subsystem, the dynamics of the solenoid are assumed linear, with a constant inductance L, to facilitate the analysis. Studying only changes in input and output signal, the governing linearised equations transformed into the Laplace domain are shown in Equations (34)–(36), where s is the Laplace operator and Δ indicates a change in the signal.

$$\Delta is = \frac{1}{L}\left(\Delta V_s - R\Delta i\right) \tag{34}$$

$$\Delta xs = \frac{1}{m}\left(K_{fi}\Delta i - A_c\Delta p - K_e\Delta x - B\Delta xs\right) \tag{35}$$

$$\Delta ps = \frac{V}{\beta}\left(K_q\Delta x - K_c\Delta p + K_{c_{ps}}\Delta p_s + A_c\Delta xs - \Delta q_l\right) \tag{36}$$

The corresponding derivatives are defined in the appendix. A block diagram can be derived from the linearised equations, shown in Figure 6. The hydro-mechanical feedback appears and it is also seen that the solenoid dynamics do not affect the loop gain in the simplified case. The frequency response of the loop gain is shown in Figure 7 for two working points, corresponding to two points along the static pressure-flow curve at 70% duty cycle. The two points are defined in Table 1. The first working point is where the pressure is declining with the flow. The second point is where the pressure is increasing with the flow, yielding negative characteristics. The linearized system is stable in both cases, which agrees with observations of the physical system. In the second case, however, the phase margin begins at −180° since the linearised spring constant, K_e, is negative. Being quite low, the spring constant only affects the system at very low frequencies, allowing the system to maintain a positive, but low, phase margin at the crossover frequency. It can be noted that the resulting pumping motion of the spool can be ignored due to the very high frequency.

6. Results

This section presents the results from measurements and simulations of the solenoid and the complete valve.

6.1. Solenoid

The static characteristic of the solenoid, represented as force vs. position at different current levels, is shown

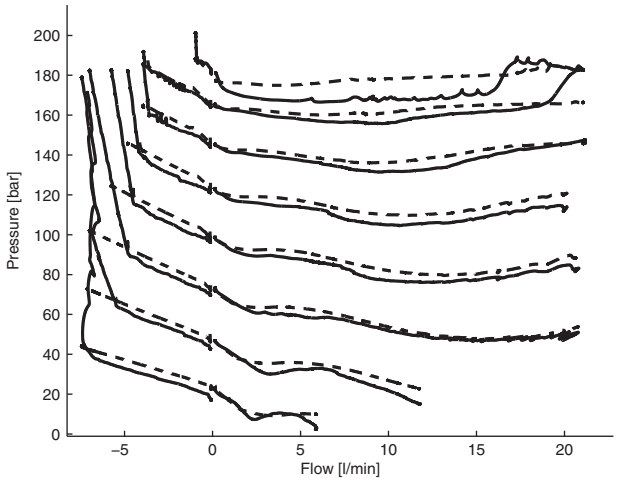

(a) Pressure vs. flow curves of the valve

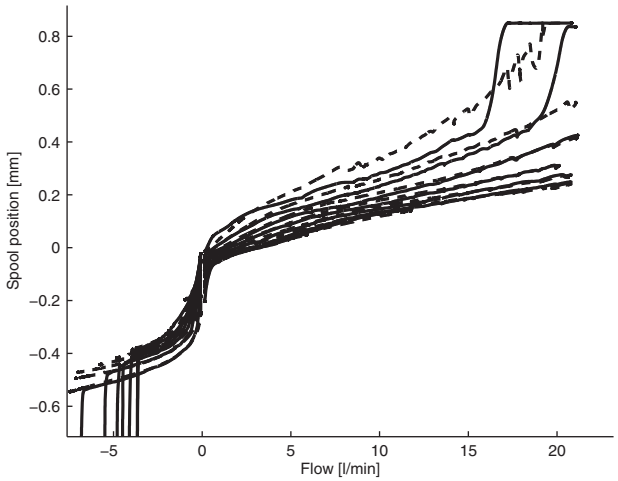

(b) Position vs. flow of the valve

Figure 10. Comparison between measured (solid) and simulated (dashed) static characteristics of the valve.

in Figure 8. The small variation in resistance during the measurements has been taken into account in the figure.

Figure 9 shows the comparison of between measured and simulated solenoid characteristic and performance. Although validation has been performed over the entire working range, the figure shows the results at the valve's corresponding centre position. The results for flux linkage are presented at the extreme positions to show the variation over the stroke. The coil resistance was calculated at stationary points in order to compensate for its variation.

6.2. Valve

Static characteristics

Figure 10 shows the comparison of the static characteristics of the valve between measured and simulated results. The measurements were taken at 30% - 100% duty cycles, in steps of 10%. Figure 10(a) shows the pressure vs. flow characteristics and Figure 10(b) shows the position of the magnet core vs. the flow.

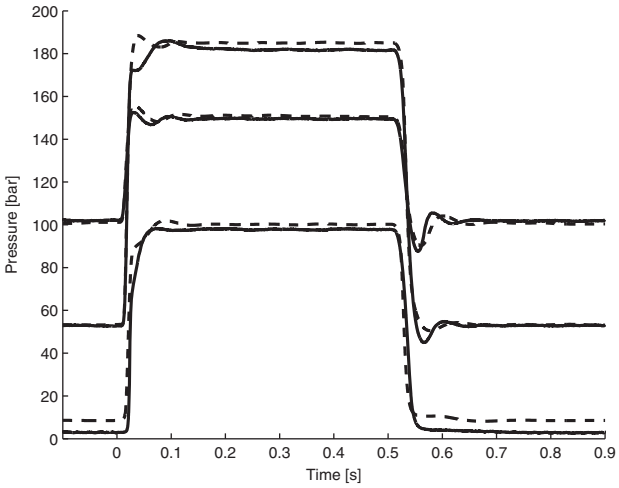

(a) Pressure response of the valve

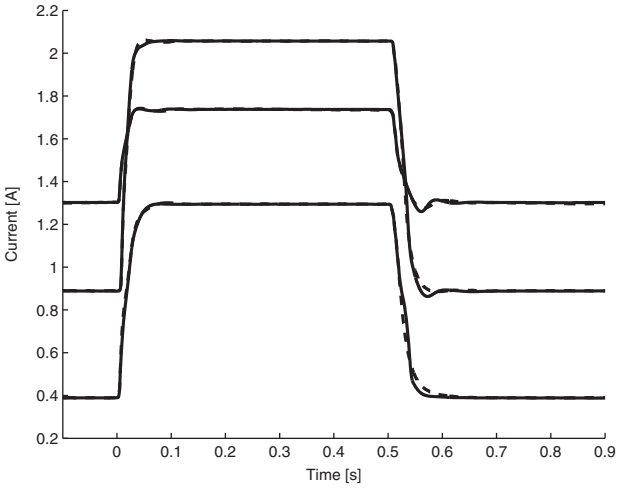

(b) Current response of the valve

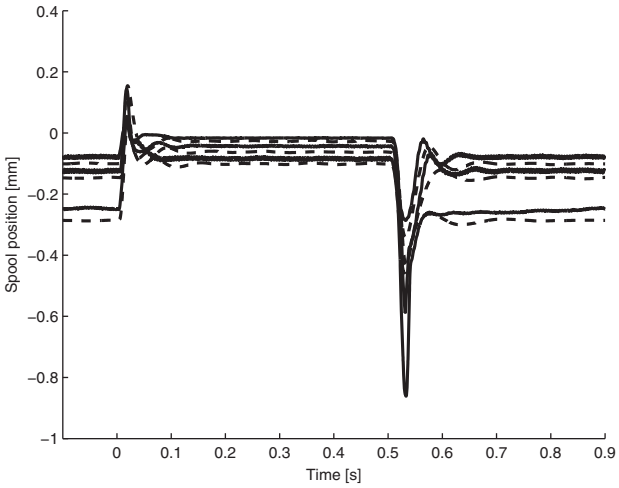

(c) Position response of the valve

Figure 11. Comparison between measured (solid) and simulated (dashed) dynamic performance of the valve.

Dynamic characteristics

Figure 11 shows the performance of the valve for step signal input at different levels and amplitudes. The responses are compared to simulation results. Performance is measured for pressure, current, and magnet core position.

7. Discussion

There are some remarks regarding the results that should be discussed. First of all, the discharge coefficient compensates for the fact that the actual cross-sectional area of the stream is different to the area opening of the valve. This means that the discharge coefficient contains the uncertainties regarding the modelling of the area opening. There are uncertainties regarding the possible underlap or overlap of the spool and the gap between the spool and the spool body. The flow path of the leakage is also unknown but assumed to follow a certain direction and this will also affect the shape of the discharge coefficient. Nevertheless, the discharge coefficient clearly shows how the flow transfers from laminar in the gap region towards turbulent flow. The shape of the curve is also similar to the literature, Merritt (1967).

The flow forces very much define the static characteristic of the valve. Since it was not possible to measure the actual flow forces, the accuracy of the flow force model can not be confirmed. It is also subject to modelling errors since it also depends on the discharge coefficient. The complete model, nonetheless, accurately describes the behaviour of the valve. Since the mechanical spring is very weak, the force balance on the spool is very sensitive to any disturbances in the flow path that can affect the flow jet angle.

Overall, the simulation results agree well with the measurements for all states of the valve, pressure, current and spool position, which suggests that the model has captured the essential behaviour of the valve.

The linearised analysis suggests that the effective spring constant is negative in the phase where the pressure increases with flow in reducing mode. This is reasonable since the pressure-flow curve changes direction. The negative spring constant only affects the system in the low-frequency region and stability is therefore maintained.

8. Conclusions

The modelling procedure for a solenoid pressure control valve with negative characteristic has been realised with very good agreement. This was accomplished through an accurate modelling of both the orifice flow and the flow forces acting on the spool. The orifice flow takes into account the change in flow type, from a laminar to a turbulent flow, while the flow force model also takes into account how the jet flow angle changes over the stroke.

It can be seen from the derived model that the main cause of the negative characteristic is that the flow stream changes direction with spool stroke to such an extent that the flow force actually decreases with increased flow, causing a rise in pressure. In a linearised sense, this turns out as negative effective spring constant dominating the low-frequency region.

Nomenclature

Parameter	Description	Unit
m:	Total mass of moving parts	kg
i:	Current	A
i_R:	Restoring current	A
i_d:	Dissipating current	A
A_c:	Pressure area	m^2
A_{cc}:	Damping chamber pressure area	m^2
A:	Opening area	m^2
O:	Opening circumference	m
d_h:	Hydraulic diameter	m
r:	Radius of opening holes	m
h_{gap}:	Gap height between spool and body	m
K:	Spring stiffness	N/mm
f_0	Pretension force	N
B:	Viscous friction coefficient	Ns/m
F_s:	Solenoid force	N
F_f:	Flow force	N
x:	Spool position	mm
v:	Spool velocity	m/s
p:	Pressure	Pa
p_c:	Pressure in damping chamber	Pa
V:	Load volume	m^3
V_c:	Volume in damping chamber	m^3
q_v:	Valve flow	m^3/s
q_l:	Load flow	m^3/s
q_c:	Damping chamber flow	m^3/s
V_s:	Total voltage	V
V_R:	Resistive voltage	V
V_L:	Inductive voltage	V
R:	Coil resistance	Ω
ρ:	Density	kg/m^3
β:	Bulk modulus	Pa
δ:	Jet flow angle	[rad]
ν:	Kinematic viscosity	m^2/s
λ:	Flux linkage	W_b
f_1:	Function coefficient	$A/(W_b^3)$
f_2:	Function coefficient	$A/(W_b^2)$
f_3:	Function coefficient	A/W_b
p_{f11}:	Function coefficient	$A/(W_b^3 m^5)$
p_{f12}:	Function coefficient	$A/(W_b^3 m^4)$
p_{f13}:	Function coefficient	$A/(W_b^3 m^3)$
p_{f14}:	Function coefficient	$A/(W_b^3 m^2)$
p_{f15}:	Function coefficient	$A/(W_b^3 m)$
p_{f16}:	Function coefficient	A/W_b^3
p_{f21}:	Function coefficient	$A/(W_b^2 m^5)$
p_{f22}:	Function coefficient	$A/(W_b^2 m^4)$
p_{f23}:	Function coefficient	$A/(W_b^2 m^3)$
p_{f24}:	Function coefficient	$A/(W_b^2 m^2)$
p_{f25}:	Function coefficient	$A/(W_b^2 m)$
p_{f26}:	Function coefficient	A/W_b^2
p_{f31}:	Function coefficient	$A/(W_b m^2)$
p_{f32}:	Function coefficient	$A/(W_b m)$
p_{f33}:	Function coefficient	A/W_b
p_{d_1}:	Function coefficient	A/V^3
p_{d_2}:	Function coefficient	A/V^2

p_{d_3}: Function coefficient A/V
p_{d_4}: Function coefficient A
p_{fs_1}: Function coefficient $N/(A^5)$
p_{fs_2}: Function coefficient $N/(A^4)$
p_{fs_3}: Function coefficient $N/(A^3)$
p_{fs_4}: Function coefficient $N/(A^2)$
$p_{fs_{11}}$: Function coefficient $N/(A^5m^3)$
$p_{fs_{12}}$: Function coefficient $N/(A^5m^2)$
$p_{fs_{13}}$: Function coefficient $N/(A^5m)$
$p_{fs_{14}}$: Function coefficient N/A^5
$p_{fs_{21}}$: Function coefficient $N/(A^4m^3)$
$p_{fs_{22}}$: Function coefficient $N/(A^4m^2)$
$p_{fs_{23}}$: Function coefficient $N/(A^4m)$
$p_{fs_{24}}$: Function coefficient N/A^4
$p_{fs_{31}}$: Function coefficient $N/(A^3m^3)$
$p_{fs_{32}}$: Function coefficient $N/(A^3m^2)$
$p_{fs_{33}}$: Function coefficient $N/(A^3m)$
$p_{fs_{34}}$: Function coefficient N/A^3
$p_{fs_{41}}$: Function coefficient $N/(A^2m^3)$
$p_{fs_{42}}$: Function coefficient $N/(A^2m^2)$
$p_{fs_{43}}$: Function coefficient $N/(A^2m)$
$p_{fs_{44}}$: Function coefficient N/A^2

Acknowledgements

The authors wish to thank Hydac and Nordhydraulic for donating the valves.

Disclosure statement

No potential conflict of interest was reported by the authors.

ORCID

Petter Krus http://orcid.org/0000-0002-2315-0680

Notes on contributors

Alessandro Dell'Amico received his Master of Science in Mechanical Engineering from Linköping University and is currently working towards a PhD degree at the division of Fluid and Mechatronic Systems, Linköping University. Research interest in modelling, simulation and control of fluid power systems, mechatronic systems and digital hydraulics. Applications are in automotive systems and construction machinery.

Petter Krus Professor in Fluid and Mechatronic Systems at Linköping University. Research interest in fluid power, mechanical, and mechatronic systems technology, specifically focusing on system dynamics, control, system simulation, optimization, system design and design automation. Applications are in aircraft design, road vehicles and construction machines.

References

Åman, R., Handroos, H., and Eskola, T., 2008. Computionally efficient two-regime flow orifice model for real-time simulation. *Simulation modelling practice and theory*, 16, 945–961.

Amirante, R., Vescovo, G.D., and Lippolis, A., 2006. Flow forces analysis of an open center hydraulic directional control valve sliding spool. *Energy conversion and management*, 47, 114–131.

Borghi, M., Milani, M., and Paoluzzi, R., 2000. Stationary flow force analysis on compensated spool valves. *International journal of fluid power*, 1 (1), 17–25.

Borutzky, W., Barnard, B., and Thoma, J., 2002. An orifice flow model for laminar and turbulen conditions. *Simulation modelling practice and theory*, 10, 141–152.

Branciforte, M., Meli, A., Muscato, G., and Porto, D., 2011. Ann and non-integer order modeling of abs solenoid valves. *IEEE transactions on control systems technology*, 19 (3), 628–635.

Dasgupta, K., and Watton, J., 2005. Dynamic analysis of proportional solenoid controlled piloted relief valve by bondgraph. *Simulation modelling practice and theory*, 13, 21–38.

Dell'Amico, A., 2013. *Pressure control in hydraulic power steering systems*. Lic. thesis No. 1626. Linköping University.

Ellman, A., and Piché, R., 1996. A modified orifice flow formula for numerical simulation of fluid power systems. *Fluid power systems and technology*, 3, 59–63.

Erhard, M., Weber, J., and Schoppel, G., 2013. Geometrical design and operability verification of a proportional pressure relief valve. *In*: *The 13th Scandinavian international conference on fluid power, SICFP2013*, 3–5 June, Linköping, Sweden, 365–376.

Merritt, H.E., 1967. *Hydraulic control systems*. New York: Wiley.

Palmberg, J.-O., Andersson, B., and Malmros, C., 1983. Analysis and synthesis of hydraulic pressure regulators. *In*: *IASTED, international conference ACI'83*. Köpenhamn.

Vaughan, N. and Gamble, J., 1996. The modeling and simulation of a proportional solenoid valve. *Transactions of the ASME Journal of Dynamic Systems, Measurements and Control*, 118, 120–125.

Walker, P.D., Zhu, B., and Zhang, N., 2014. Nonlinear modeling and analysis of direct acting solenoid valves for clutch control. *Transactions of the ASME journal of dynamic systems, measurements and control*, 136, 051023-1–051023-9.

Wu, D., Burton, R., and Schoenau, G., 2002. An empirical discharge coefficient model for orifice flow. *International journal of fluid power*, 3 (3), 13–18.

Appendix

A.1. Linearised derivatives

The derivatives from the linearised system equations are defined below.

$$K_{fi} = \frac{\partial F_s(i_0, x_0)}{\partial i}$$
$$K_{fx} = \frac{\partial F_s(i_0, x_0)}{\partial x}$$
$$K_{ff} = \frac{\partial F_f(x_0, p_{s0}, p_0)}{\partial x}$$
$$K_e = K - K_{fx} + K_{ff}$$

$$K_q = \frac{\partial q_v(x_0, p_{s0}, p_0)}{\partial x}$$
$$K_c = -\frac{\partial q_v(x_0, p_{s0}, p_0)}{\partial p}$$
$$K_{c_{ps}} = \frac{\partial q_v(x_0, p_{s0}, p_0)}{\partial p_s}$$

A.2. Parameter values

Table 1. Parameter values

Parameter	Value	Unit
$p_{f_{11}}$	-69.18	$A/(W_b^3 m^5)$
$p_{f_{12}}$	335.12	$A/(W_b^3 m^4)$
$p_{f_{13}}$	-449.62	$A/(W_b^3 m^3)$
$p_{f_{14}}$	99.99	$A/(W_b^3 m^2)$
$p_{f_{15}}$	36.65	$A/(W_b^3 m)$
$p_{f_{16}}$	324.00	A/W_b^3
$p_{f_{21}}$	15.23	$A/(W_b^2 m^5)$
$p_{f_{22}}$	-72.02	$A/(W_b^2 m^4)$
$p_{f_{23}}$	87.96	$A/(W_b^2 m^3)$
$p_{f_{24}}$	-7.55	$A/(W_b^2 m^2)$
$p_{f_{25}}$	-5,17	$A/(W_b^2 m)$
$p_{f_{26}}$	-31.69	A/W_b^2
$p_{f_{31}}$	2.13	$A/(W_b m^2)$
$p_{f_{32}}$	-9.48	$A/(W_b m)$
$p_{f_{33}}$	19.14	A/W_b
p_{d_1}	-0.0004	A/V^3
p_{d_2}	-0.0003	A/V^2
p_{d_3}	0.0472	A/V
p_{d_4}	0.0059	A
$p_{f_{s11}}$	-1.06	$N/(A^5 m^3)$
$p_{f_{s12}}$	4.30	$N/(A^5 m^2)$
$p_{f_{s13}}$	-2.30	$N/(A^5 m)$
$p_{f_{s14}}$	-1.55	N/A^5
$p_{f_{s21}}$	6.07	$N/(A^4 m^3)$
$p_{f_{s22}}$	-23.45	$N/(A^4 m^2)$
$p_{f_{s23}}$	9.16	$N/(A^4 m)$
$p_{f_{s24}}$	14.69	N/A^4
$p_{f_{s31}}$	-12.83	$N/(A^3 m^3)$
$p_{f_{s32}}$	47.77	$N/(A^3 m^2)$
$p_{f_{s33}}$	-17.55	$N/(A^3 m)$
$p_{f_{s34}}$	-41.77	N/A^3
$p_{f_{s41}}$	10.76	$N/(A^2 m^3)$
$p_{f_{s42}}$	-40.61	$N/(A^2 m^2)$
$p_{f_{s43}}$	23.38	$N/(A^2 m)$
$p_{f_{s44}}$	47.33	N/A^2
m	0.04	kg
A_c	$6.36 \cdot 10^{-5}$	m^2
A_{cc}	$6.05 \cdot 10^{-5}$	m^2
r	$1.5 \cdot 10^{-3}$	m
h_{gap}	$1.5 \cdot 10^{-5}$	m
K	0.5	N/mm
f_0	2	N
B	4.47	Ns/m
$B_{simplied}$	223.6	Ns/m
V	$1 \cdot 10^{-4}$	m^3
V_c	$4.7 \cdot 10^{-11}$	m^3
ρ	900	kg/m^3
β	$1 \cdot 10^9$	Pa
ν	$46 \cdot 10^{-6}$	m^2/s
K_d	$1.24 \cdot 10^{-11}$	m^5/Ns